Energy Storage Materials 8 (2017) 28–34

Contents lists available at ScienceDirect

Energy Storage Materials

journal homepage: www.elsevier.com/locate/ensm

Self-templated synthesis of N-doped $CoSe_2$/C double-shelled dodecahedra for high-performance supercapacitors

Yifang Zhang[a], Anqiang Pan[a,*], Yaping Wang[a], Xinxin Cao[a], Zilong Zhou[b], Ting Zhu[a], Shuquan Liang[a,*], Guozhong Cao[c,*]

[a] School of Materials Science and Engineering, Central South University, Changsha 410083, Hunan, China
[b] School of Resources and Safety Engineering, Central South University, Changsha 410083, Hunan, China
[c] Department of Materials Science and Engineering, University of Washington, Seattle, WA 98195, United States

ARTICLE INFO

Keywords:
Nitrogen-doped carbon
Cobalt selenide
Double-shell
Metal-organic frameworks
Supercapacitors

ABSTRACT

Transition metal chalcogenides have attracted increasing attentions as electrode materials for energy storage devices. Their electrochemical properties are largely determined by morphologies and structures. In this paper, we reported the fabrication of $CoSe_2$/C dodecahedra with tunable interior structures, such as solid, yolk-shell, and double-shell structured interiors. Dodecahedron-shaped cobalt-organic frameworks are used as the sacrificial template, in which the cobalt species react with selenium to *in situ* form $CoSe_2$ nanoparticles. Moreover, the organic framework is converted into nitrogen-doped carbon framework. The controllable preparation of $CoSe_2$/C composite with diversified interior structures can be realized by a temperature determined annealing process in argon atmosphere. In particular, the unusual double-shell structured composites with non-spherical shells and heterogeneous intervals are formed. The possible formation mechanism of the structure is proposed. As electrode materials for supercapacitors, the double-shelled $CoSe_2$/C composites exhibit high capacitance, good rate capability and long-term cycling stability.

1. Introduction

Transition metal chalcogenides have received considerable attentions over the past decades as pseudo-capacitive active materials. Among them, transition metal oxides (TMOs) [1–4], and transition metal sulfides (TMSs) [5,6], are mostly studied electrode materials due to their high capacitance and good rate capability. Transition metal selenides, with higher conductivity than their counterparts (TMOs or TMSs), are also potential candidates in energy storage and conversion systems. Many efforts have been devoted on the exploration of transition metal selenides for energy storage applications [7–9]. The structure of electrode materials should be optimized before achieving desired electrochemical performances [10–12]. In general, nanostructured electrode materials with small particle size, large specific surface area, good structural stability and high electron conductivity are preferred. In this consideration, making active substances with conductive materials are widely studied [13–15].

Among the transition metal selenides, cobalt selenides have been utilized as electrode materials for supercapacitors. To date, many delightful results have been reported for their composites. For example, cobalt selenides are grown on the supportive substrates, such as carbon cloth and carbon fiber paper [16,17]. However, the fabrication of selenides within porous carbon framework to form a coherent composite is much less reported. In these structures, active selenides are not exposed directly to the electrolyte, and the porous conductive scaffold can provide fast electron transportation and accommodate the volume changes upon repeated cycling. It is thus believed that enhanced electrochemical performance can be delivered for the coherent composite electrode materials.

Metal-organic frameworks (MOFs) derived materials have attracted increasing attentions recently as electrode materials in energy storage fields [18–21]. MOFs are chemical composed of well-organized metal centers and organic linkers. The diversified MOFs can serve as sacrificial templates for synthesizing various porous transition metal oxides after annealing in air, such as Co_3O_4 concave nanocubes [22], spindle-like Fe_2O_3 [23], CuO octahedral [24], etc. Furthermore, the organic linkers within the MOFs can be converted into carbon frameworks after annealing and carbonization in inert atmosphere. More recently, many works have been endeavored on the fabrication of transition metal chalcogenides and MOFs derived carbon composite to improve the electrochemical performance [25–27]. Although plentiful results have been obtained for transition metal oxides or transition

* Corresponding authors.
E-mail addresses: pananqiang@csu.edu.cn (A. Pan), lsq@csu.edu.cn (S. Liang), gzcao@u.washington.edu (G. Cao).

http://dx.doi.org/10.1016/j.ensm.2017.03.005
Received 13 November 2016; Received in revised form 6 February 2017; Accepted 10 March 2017
Available online 11 March 2017

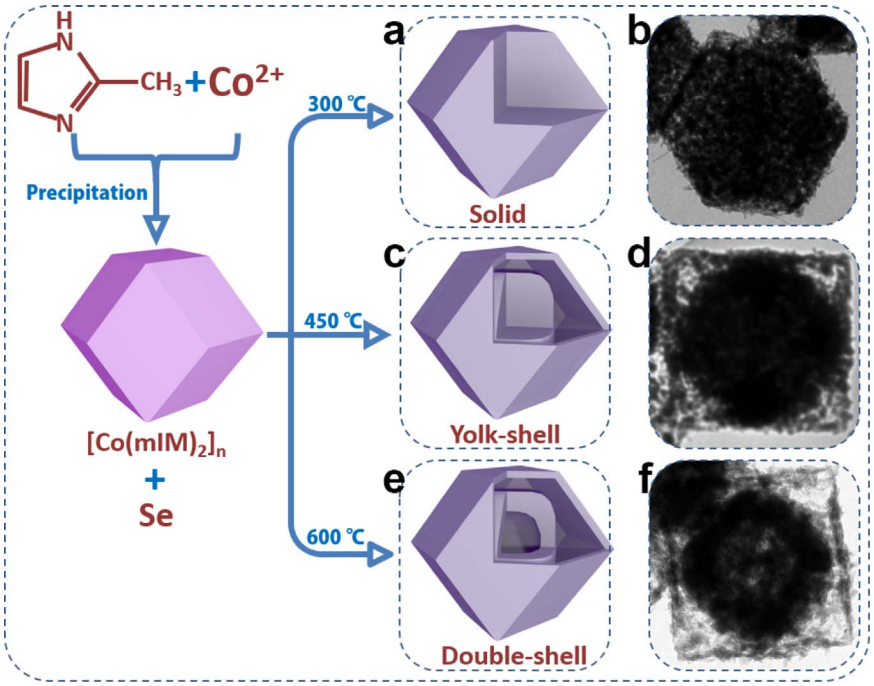

Fig. 1. Schematic illustration of the preparation process of solid (a, b), yolk-shelled (c, d) and double-shelled (e, f) $CoSe_2$/C composite.

metal sulfides, much less work is reported for transition metal selenides [28]. Moreover, the controllable preparation of transition metal selenides and carbon composites with diversified interior structures is rarely reported.

Herein, we report the controllable preparation of $CoSe_2$/C dodecahedra with solid, yolk-shelled and double-shelled structures using MOFs as sacrificial templates. The formation process is carefully studied and the possible mechanism is proposed. Moreover, the $CoSe_2$ nanoparticles are *in situ* embedded in the MOFs-derived nitrogen-doped carbon matrix. As electrode materials for supercapacitors, the double-shelled $CoSe_2$/C hollow dodecahedra exhibit high specific capacitance, superior rate capability and cycling stability.

2. Experimental section

2.1. Synthesis of cobalt organic framework

All the solvents and chemicals were used of reagent grade without further purification. Cobalt organic framework (ZIF-67) was prepared via a precipitation reaction. In a typical synthesis, 4 mmol of cobalt nitrate hexahydrate and 20 mmol of 2-methylimidazole were dissolved into 100 mL of methanol, separately. The two solutions were then mixed uniformly before being stood for 24 h. The ZIF-67 with large size was synthesized using 1 mmol of cobalt nitrate hexahydrate and 5 mmol of 2-methylimidazole added separately into 50 mL of methanol. The above two solutions were mixed and then incubated for 24 h. ZIF-67 crystals with the formula $[Co(mIM)_2]_n$ were incubated during this process. Afterwards, the solid products were collected by centrifugation and washed with ethanol for several times, followed by drying in vacuum at 50 °C.

2.2. Synthesis of $CoSe_2$/C dodecahedra

The as-prepared ZIF-67 and selenium powder were grounded together with a mass ratio of 1:1 before annealing at 300, 450 or 600 °C for 4 h in a tube furnace under an argon gas flow. The temperature ramping rate was 5 °C min^{-1}. Moreover, the effects of other mass ratios (1:0.35 or 1:0.7) or the particle size of the templates on the phases and structures of the samples synthesized at 600 °C were also investigated.

2.3. Materials characterization

The crystal structures of the products were determined by powder X-ray diffraction (XRD, Rigaku D/max 2500, Cu Kα radiation, λ=1.54178 Å). The morphologies and structures of the samples were characterized by scanning electron microscopy (SEM, Nova NanoSEM230) and transmission electron microscopy (TEM, Titan G2 60-300 with image corrector). The thermogravimetric analysis (TGA, NETZSCH STA 449C) was conducted under argon atmosphere. The X-ray photoelectron spectroscopy (XPS) was performed on ESCALAB 250Xi (ThermoFisher-VG Scientific, Britain). The Raman spectroscopy measurements were performed on LabRAM Hr800 with a back illuminated charge coupled detector (CCD) attachment. Nitrogen adsorption-desorption measurements were conducted on NOVA 4200e (Quantachrome Instruments) at 77 K.

2.4. Electrochemical measurement

The $CoSe_2$/C composites with various interiors, acetylene black and polyvinylidene fluoride (PVDF) in a weight ratio of 80:10:10 were dispersed in an N-methyl-2-pyrrolidone (NMP) solution to form slurry, which was coated on a piece of clean Ni foam substrate with 1×2 cm^2 in size and dried in vacuum at 60 °C overnight. The mass loading of the electrode materials was about 1 mg cm^{-2}. The electrochemical measurements were carried out in a three-electrode system with a Pt foil counter electrode and Hg/Hg_2Cl_2, KCl (sat.) (saturated calomel electrode, SCE, 0.242 V vs. NHE) reference electrode in 2 M KOH aqueous solution as the electrolyte. Cyclic voltammetry (CV) was tested with an electrochemical workstation (CHI660C, China) at different scan rates in the voltage range of 0–0.55 V.

3. Results and discussion

Fig. 1 illustrates the formation process of $CoSe_2$/C composites with different interior structures from ZIF-67. The ZIF-67 template is prepared by a precipitation method from cobalt nitrites and 2-methylimidazole [29], and exhibits dodecahedral morphology. The

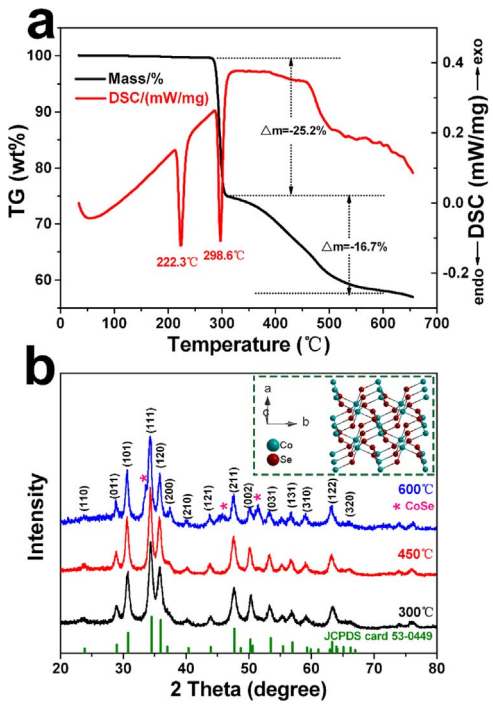

Fig. 2. (a) TG and DSC curves of the mixture of ZIF-67 and Se powders. (b) XRD patterns of the $CoSe_2$/C composite synthesized at different temperatures.

XRD pattern of ZIF-67 corresponds well with the simulated result (Fig. S1a) and previous report [30], demonstrating the successful formation of ZIF-67. The as-synthesized templates are uniform dodecahedra with a mean size of 500 nm (Fig. S1b). The ZIF-67 templates also serve as the cobalt and carbon sources. After annealing with selenium powder in argon atmosphere at 300 °C, 450 °C or 600 °C for 4 h, the $CoSe_2$/C dodecahedra with solid, yolk-shelled or double-shelled structures can be obtained, respectively. Solid interior is formed at relatively low temperature of 300 °C (Fig. 1a and b). At higher temperature of 450 °C (Fig. 1c and d), the exterior dodecahedral shell can be reserved, however, an interior core appears in the dodecahedron, forming the yolk-shelled structure. Interestingly, a double-shelled structure can be obtained by further increasing the annealing temperature to 600 °C (Fig. 1e and f).

Fig. 2a shows the TG analysis and DTA result of the mixture of ZIF-67 and Se powder in argon atmosphere. The endothermic peaks at 222 °C and 298 °C are attributed to the selenium melting [31] and the reaction between ZIF-67 and Se liquid to form $CoSe_2$, respectively. The assumption is confirmed by the XRD result of the products obtained at 300 °C (Fig. 2b), which indicates the ready formation of orthorhombic $CoSe_2$ (JCPDS no. 53-0449: *Pnnm*(58), a=4.85 Å, b=5.827 Å, c=3.628 Å). The continuous weight loss thereafter can be attributed to the decomposition of the organic ligands of ZIF-67 and the evaporating of extra selenium. As shown in Fig. 2b, stable $CoSe_2$ phase can be obtained at 300 °C and 450 °C. Further increasing the annealing temperature to 600 °C, a small amount of CoSe phase appears. Thus, the whole preparation process was carried out below 600 °C.

Fig. S2 shows the SEM and TEM images of the $CoSe_2$ dodecahedra prepared at 300 °C and 450 °C. According to the SEM images, the dodecahedron-shape of the templates can be well preserved with similar size of around 500 nm for both of the annealed products (Fig. S2a and c). However, the dodecahedra have rough and porous surface compared with the ZIF-67 template. The TEM image indicates the homogeneous interior structure of the dodecahedra synthesized at 300 °C, which is composed of porous structures (Fig. S2b). For the $CoSe_2$ dodecahedra obtained at 450 °C, the porous feature of the surface is more obvious. Moreover, the broken dodecahedra in Fig. S2c reveal the empty space between the exterior shell and interior core. The TEM image (Fig. S2d) gives much clearer information about the interior of the dodecahedra. The empty space created is mainly at the corner part of the dodecahedra and the interior core is still with porous structures. The formation of the porous structures for $CoSe_2$ synthesized at 300 °C and 450 °C can be both attributed to the decomposition of organic species from the ZIF-67 templates.

Fig. 3 shows the structural characterization of $CoSe_2$ obtained at 600 °C. According to the SEM images (Fig. 3a and b), the $CoSe_2$ is also of high porosity and with similar size to the above mentioned two samples. In Fig. 3c, the TEM image further confirms that the polyhedrons are constructed by nanoparticles with diameters of about 20 nm. However, a hollow interior is created within the inner core, thus forming a double-shelled structure for the $CoSe_2$ dodecahedra. The dodecahedral exterior shell is about 500 nm in size, and the inner shell is about 300 nm. The structure can be treated as the further creation of hollow interior within the core obtained at 450 °C. The formation of this double-shelled structure with heterogeneous intervals is unusual. The HRTEM image (Fig. 3d) displays the fringe spacing of 0.26 nm, in good agreement with the planar distance of (111) plane of $CoSe_2$. The elemental mapping results (Fig. 3e) obtained by HAADF technique demonstrate the homogeneous distribution of Co, Se, C and N elements. The Raman spectrum of the $CoSe_2$/C composite shows two broad peaks at around 1350 cm^{-1} and 1570 cm^{-1}, which can be attributed to the characteristic D and G bands for carbon, respectively (Fig. S3) [32–34]. The area ratio of I_D/I_G is around 2.6, implying the carbon framework is with low graphitization degree because the annealing temperature is just 600 °C.

Based on above results, the possible formation mechanism is postulated as follows: At relative low temperature (< 300 °C), the decomposition of ZIF-67 happens gently. The selenium diffuses into ZIF-67 and reacts with cobalt gradually to form a homogeneous $CoSe_2$ interior. However, the decomposition of the organic species in the ZIF-67 and the selenylation between cobalt and selenium are much tense at higher temperature (450 °C). The cobalt species near the surface diffuse outward to react with selenium to form $CoSe_2$ firstly, and the interior material contract inside to form the empty gap between the exterior shell and the mesoporous core. Thereafter, the selenium diffuse inside and react with the remaining core material. During this process, the round shaped core is formed, while the dodecahedron-shaped exterior is preserved. At the annealing temperature of 600 °C, the outward diffusion of cobalt species in the inner core and reaction with the coming selenium further create the hollow interior, forming the double-shelled $CoSe_2$/C hollow dodecahedra. In the reaction process, abundant selenium is needed to ensure the formation of the double-shelled structure. We have used ZIF-67 and Se powder with mass ratio of 1:0.35 or 1:0.7 to synthesize the cobalt selenide. The mass ratios are designed based on the approximate molar ratio of $Co(mIM)_2$ and Se (1:1 or 1:2 for mass ratio of 1:0.35 or 1:0.7). Fig. S4 shows the structural characterization results for these samples. According to the XRD results, the cobalt species are not fully selenized. Although the core-shelled structure can also be obtained, only the product using more selenium reactants can get a double-shelled structure. Moreover, the diffusion of selenium into the dodecahedra is also important to form the double-shelled structure. As shown in Fig. S5, the annealed product is composed of the mixed phases of $CoSe_2$ and CoSe with porous solid interiors when larger ZIF-67 templates with size of around 2 μm are annealed with abundant selenium at 600 °C. At high temperatures, some selenium evaporates before diffusing into the thick wall of the larger ZIF-67 template. Thus the annealing temperature, the sufficient selenium, and the easy diffusion of selenium are all important factors for the formation of the double-shelled structure.

X-ray photoelectron spectroscopy (XPS) was employed to further investigate the chemical composition of the $CoSe_2$/C composite. The survey spectrum shown in Fig. S6 indicates the presence of C, N, Co and Se elements in the composite. The O element is detected owing to

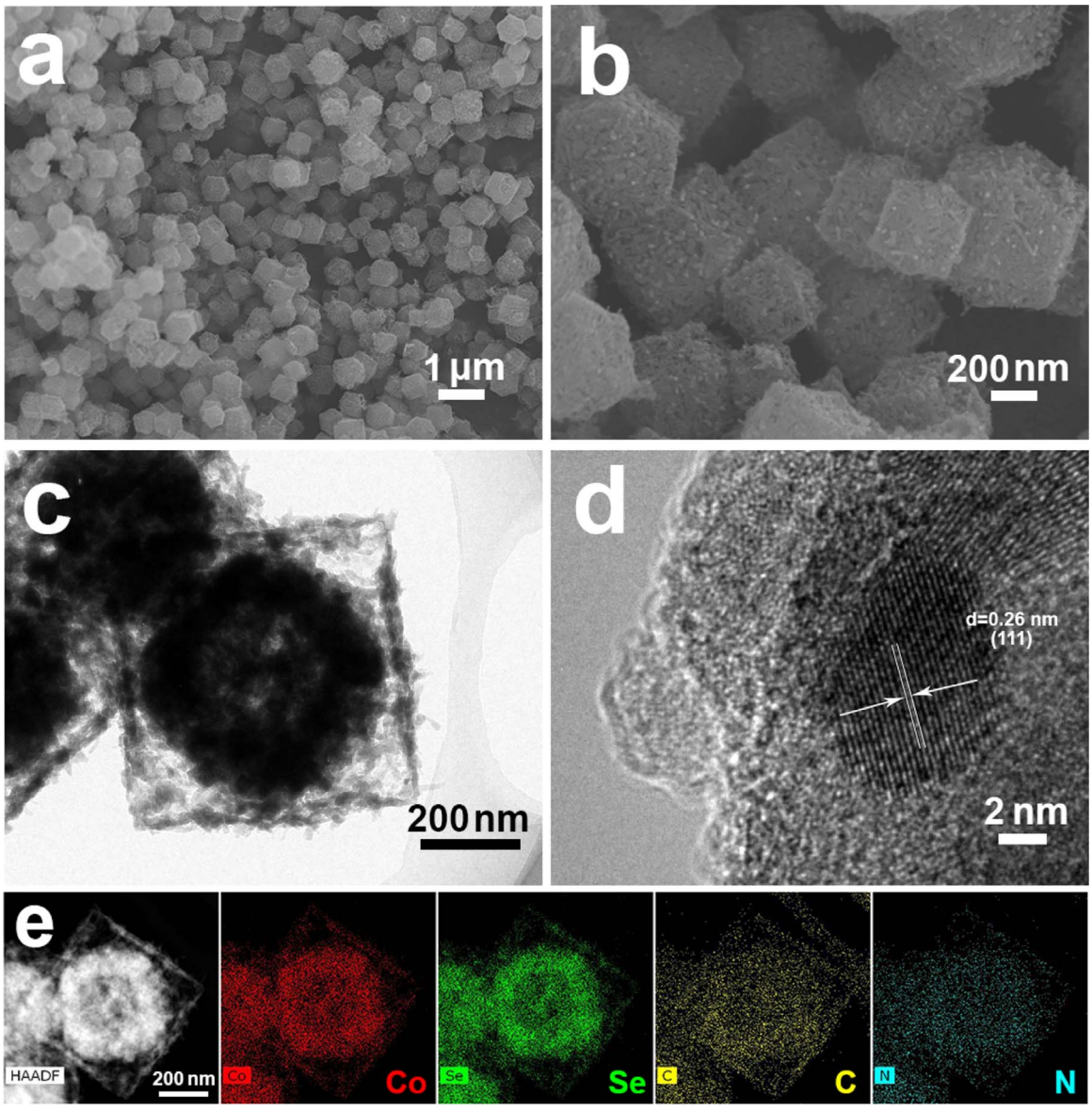

Fig. 3. SEM (a, b), TEM (c), HRTEM (d) and elemental mapping images (e) of the double-shelled $CoSe_2$/C composite.

the exposure to the air. The high-resolution XPS spectra of C 1s in Fig. 4a display peaks at 284.3, 285.4 and 286.9 eV, which can be attributed to the sp^2 C, N–sp^2 C and N–sp^3 C bonds, respectively [35], demonstrating the carbon is nitrogen-doped. The existence of N element can be further verified by the N 1s spectrum (Fig. 4b). The spectrum shows the composite contains nitrogen atoms in different oxidation states, including pyridinic N, pyrrolic N and graphitic N with binding energies of 398.4, 399.6 and 400.7 eV, respectively [35,36]. For the Co 2p spectrum shown in Fig. 4c, peaks at 780.7 and 796.6 eV correspond to Co $2p_{3/2}$ and Co $2p_{1/2}$, respectively. The energy difference of ΔE=15.9 eV between the two peaks is close to the value for CoO (ΔE=15.5 ± 0.1 eV), implying the Co species exist as Co^{2+} ion, not Co (ΔE=15.05) [37]. These peaks can be assigned to Co-Se because the valence state of Co is Co^{2+} both in $CoSe_2$ and CoSe. The peaks at 785.6 and 802.2 eV are the satellite peaks of Co 2p [38]. Pyridinic N and pyrrolic N can both coordinate with Co, so the peaks at 781.8 and 797.8 eV may be assigned to Co-N_x structures [39–42]. The small peak at 778.1 eV corresponds to Co-O_x bond caused by the partial surface oxidation [38]. Considering the existence of both Se^- and Se^{2-}, the fitted results of Se 3p are shown in Fig. 4d [43]. The valences of Se are Se^- or Se^{2-} for $CoSe_2$ or CoSe, respectively. The Se $3p_{3/2}$ peak can be divided into two peaks located at 164.6 and 161.7 eV, which can be assigned to $CoSe_2$ and CoSe, respectively. The Se $3p_{1/2}$ peak can be divided into two peaks at 170.2 and 167.2 eV, also assigned to $CoSe_2$ and CoSe, respectively. These results indicate the existence of a small amount of CoSe in the double-shelled $CoSe_2$/C composite. The nitrogen heteroatoms in the carbon matrix are considered favorable for improving the electronic conductivity and creating more active sites [44–46]. Furthermore, the nitrogen doping will provide strong bonding with the hybrid material, leading to high stability of the composite [47,48].

Nitrogen adsorption-desorption analyses were carried out to further study the porous structure of the $CoSe_2$/C dodecahedra with different interior structures. As shown in Fig. S7a, the curves are all type-IV isotherms with type-H3 hysteresis loops in the relative pressure range of 0.5–1.0 P/P_0, indicating the mesoporous structure of the samples [49]. According to Brunauer-Emmett-Teller (BET) method, the $CoSe_2$/C composites present surface area of 64.5, 93.5 and 109.4 $m^2\ g^{-1}$ for the solid, yolk-shelled and double-shelled samples, respectively. Fig. S7b shows the pore-size distribution of the $CoSe_2$/C composites calculated by the Barrett-Joyner-Halenda (BJH) method. The majority of pores are less than 10 nm. The double-shelled $CoSe_2$/C has the largest surface areas and pore volumes compared with

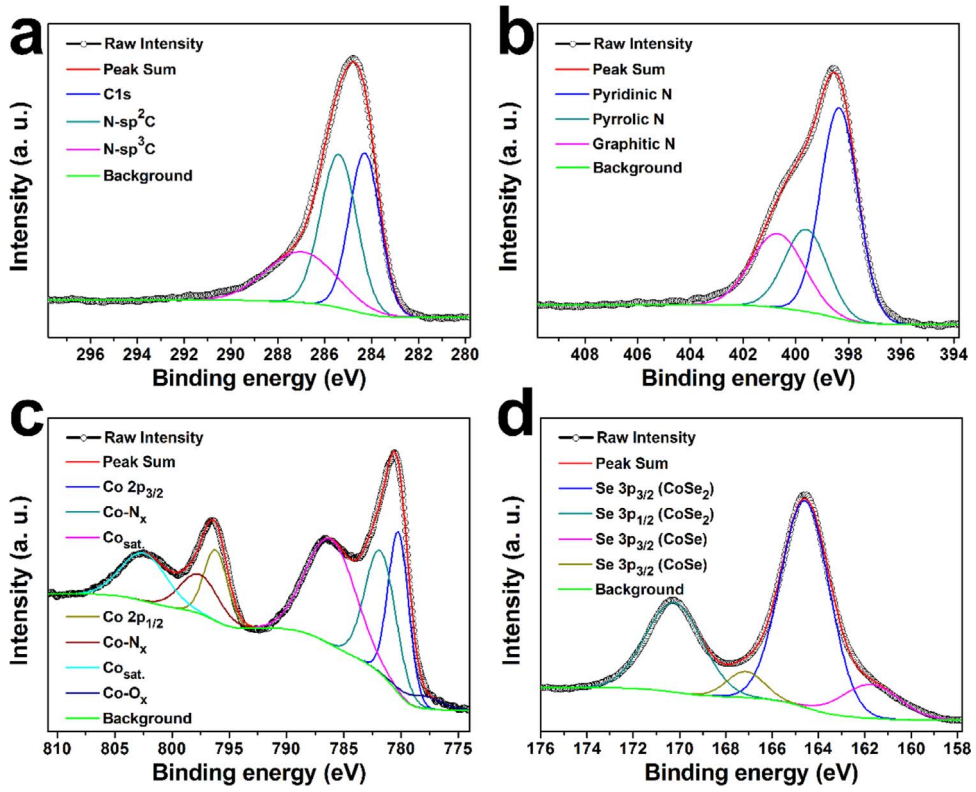

Fig. 4. High-resolution XPS spectra of (a) C 1s, (b) N 1s, (c) Co 2p, and (d) Se 3p for the double-shelled $CoSe_2$/C composite.

the other samples. The high surface areas with suitable pore-size distribution can provide abundant mesopores as ion reservoirs and shorten the diffusion length for charge carriers in the redox reactions [50].

The $CoSe_2$/C dodecahedra were assembled into supercapacitors to evaluate their electrochemical performances and the results are shown in Fig. 5. Fig. 5a shows the cyclic voltammograms (CV) of the $CoSe_2$/C composites with different interiors at a scan rate of 20 mV s^{-1}. Typical redox peaks are all presented for the CV curves. The observations are similar to the previously reported results for cobalt oxides and sulfides

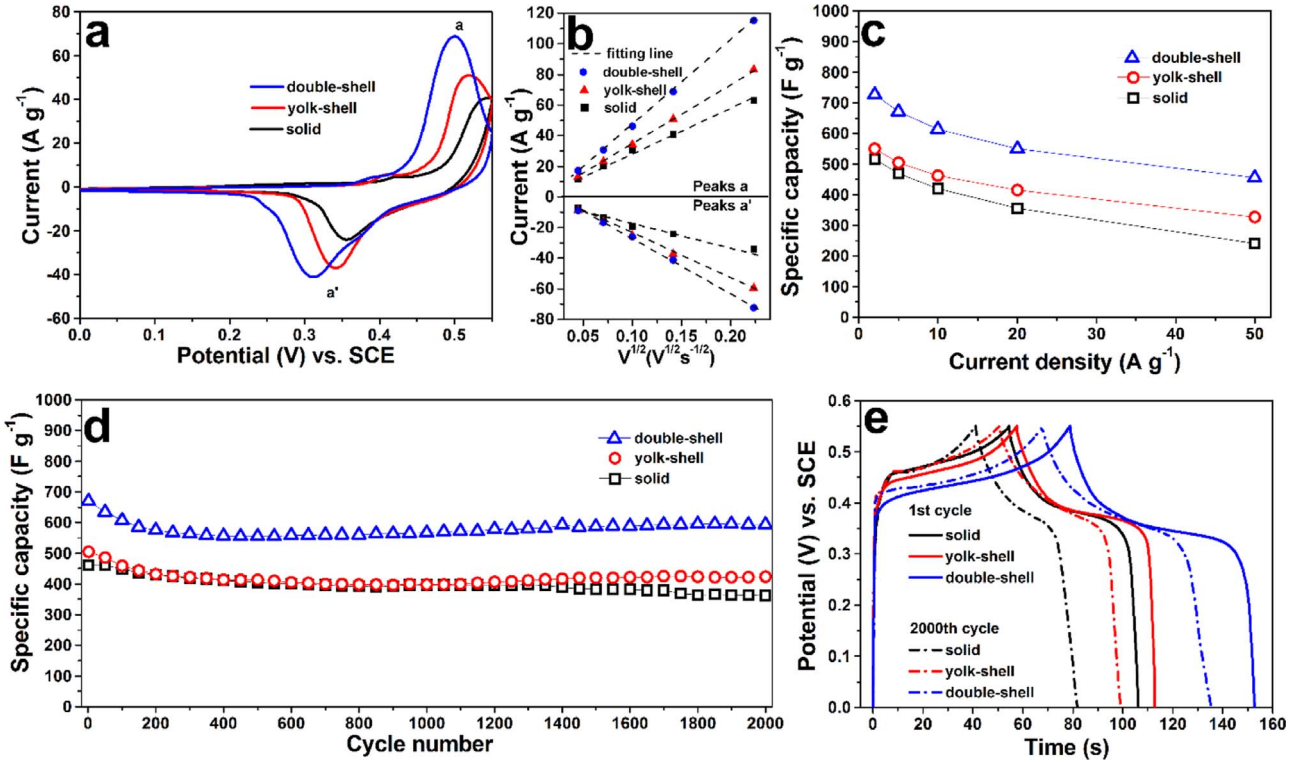

Fig. 5. Cyclic voltammogram at 20 mV s^{-1} (a), the linear fitting of I_p vs $v^{1/2}$ curves for the redox peaks a and a' (b), specific capacitances at different current densities (c), cycling performance at 5 A g^{-1} (d), the first and 2000th charge-discharge curves at current density of 5 A g^{-1} (e) for the $CoSe_2$/C composite with different interiors.

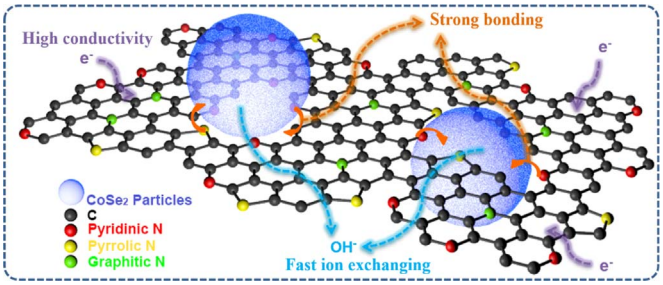

Fig. 6. Schematic illustration of the $CoSe_2$/nitrogen-doped carbon composites with fast ion exchanging, high conductivity, and strong bonding between the composites.

[50–52]. The electrochemical capacitance of $CoSe_2$/C may be attributed to the Co^{2+}/Co^{3+} and Co^{3+}/Co^{4+} redox couples, and mediated by OH^- ions in the alkaline electrolyte. As shown in Fig. 5a, the current densities of the $CoSe_2$/C dodecahedra are in the order of double-shelled ones > yolk-shelled ones > solid ones, which indicates the highest pseudocapacitance of the double-shelled $CoSe_2$/C [53]. The CV curves at different scan rates for the three samples are shown in Fig. S8. The peak currents at different scan rates for all three $CoSe_2$/C samples are plotted in Fig. 5b. It shows that the corresponding peak current has a linear relationship with the square root of scan rate, indicating the good reversibility of hydroxyl-ion diffusion-controlled faradic reaction of the $CoSe_2$/C composites [5,17,54]. However, the fitting line for the double-shelled electrode has a bigger slope compared to the other two samples, which suggests its faster reaction at high rates. The galvanostatic charge and discharge curves at different current densities ranging from 2 to 50 A g^{-1} are shown in Fig. S9. The specific capacitances of the electrodes can be calculated based on the charge-discharge test and Eq. (1):

$$C = \frac{I\Delta t}{M\Delta V} \tag{1}$$

where C (F g^{-1}) is the specific capacitance, I (A) is the discharge current, Δt (s) is the discharging time, ΔV (V) is the voltage window, and M (g) is the mass of active materials. Fig. 5c shows the capacitances of the electrodes at different current densities. For the double-shelled $CoSe_2$/C, high pseudocapacitances of 726, 671, 615, 549, and 455 F g^{-1} can be obtained at 2, 5, 10, 20, and 50 A g^{-1}, respectively. Fig. 5d displays the long-term cyclic stability of the electrodes at the current density of 5 A g^{-1}. Although the double-shelled electrode exhibits a capacity decay from 669 to 575 F g^{-1} in the first 200 cycles, the capacitance increases gradually to 618 F g^{-1} during the following cycles, which may be attributed to the full activation of the electrode [55]. All three samples present good rate performance and cyclic stability, implying the merits of constructing $CoSe_2$ nanoparticles in the nitrogen-doped carbon frameworks. However, the capacitances of electrode with double-shelled interiors are much higher than those of the solid or yolk-shelled ones. This can be attributed to the largest surface areas and pore volumes of the double-shelled sample, which provide more active site for redox reactions. Fig. S10 shows the cycling behavior of the double-shelled sample at 10 A g^{-1}. About 84.7% of its original specific capacitance can be retained after 5000 cycles, demonstrating the good electrochemical stability of the double-shelled $CoSe_2$/C hollow dodecahedra. The electrochemical performance of the CoSe/C sample obtained by annealing ZIF-67 and Se powder with mass ratio of 1:0.35 at 600 °C is provided in Fig. S11. Fig. S11a shows the CV curves at different scan rates. Fig. S11b and c show the charge/discharge curves at different current densities and the calculated capacitances of the yolk-shelled CoSe/C sample. Capacitances of 658, 614, 562, 480, and 318 F g^{-1} can be obtained at the current densities of 2, 5, 10, 20, and 50 A g^{-1}, respectively. Owing to its lower molecular mass, CoSe is expected to have larger capacitance than $CoSe_2$. Although the capacitances of CoSe/C are higher than the solid or yolk-shelled $CoSe_2$/C samples, they are lower than the double-shelled $CoSe_2$/C composite which contains only a small amount of CoSe phase. The results indicate the good electrochemical performances can be attributed to the structural merits of the double-shelled structures. Moreover, compared with CoSe/C, the rate performance of $CoSe_2$/C is better. At 50 A g^{-1}, the double-shelled $CoSe_2$/C composite can retain 62.6% of the capacitance obtained at 2 A g^{-1}, while only 48.3% can be reserved for the yolk-shelled CoSe/C. The charge-discharge curves of the first and the 2000th cycles for three samples are compared in Fig. 5e. Despite the shortened charging-discharging time, the shapes of the charge-discharge curves remain almost the same. These results are better than previous metal selenides based nanostructures as electrode materials in three-electrode systems [17,56,57], and comparable to previous reports for cobalt based pseudocapacitors [51,58]. The superior electrochemical performance of $CoSe_2$/C can be attributed to the coherent double-shelled structure. As illustrated in Fig. 6: (1) the novel double-shelled hollow structure can provide more active surface for fast redox reactions and the pores within the carbon skeleton can efficiently improve the infiltration of electrolyte; (2) the nitrogen-doped carbon backbone with good conductivity can provide the fast electron transportation path way; (3) the formation of $CoSe_2$ nanoparticles within the MOFs derived carbon framework can improve their structural stability upon repeated cycling.

4. Conclusions

In summary, $CoSe_2$/C dodecahedra with solid, yolk-shelled and double-shelled structures are successfully synthesized with ZIF-67 as sacrificial templates. The $CoSe_2$/C composites are composed of *in situ* formed $CoSe_2$ nanoparticles confined in the nitrogen-doped carbon frameworks. In particular, the unique double-shelled $CoSe_2$/C composite with heterogeneous intervals between the two shells is successfully prepared. The formation process of this novel structure is carefully studied, which is related to the reaction temperature, the amount of selenium reactant, and the size of ZIF-67 to ensure the easy diffusion of selenium. When evaluated as electrode materials for supercapacitors, the double-shelled $CoSe_2$/C hollow dodecahedra exhibit superior pseudocapacitance performance. The remarkable electrochemical performance can be ascribed to the novel double-shelled hollow structure which provides more reactive sites, easy electrolyte penetration, fast electron transportation and good structural stability.

Acknowledgments

This work was supported by the National Natural Science Foundation of China (Grant Nos. 51374255 and 51302323), the Program for New Century Excellent Talents in University (Grant No. NCET-13-0594), the Research Fund for the Doctoral Program of Higher Education of China (Grant No. 201301621200), the Natural Science Foundation of Hunan Province, China (Grant No. 14JJ3018), and the Fundamental Research Funds for the Central Universities of Central South University (Grant No. 2016zzts026).

Appendix A. Supplementary material

Supplementary data associated with this article can be found in the online version at doi:10.1016/j.ensm.2017.03.005.

References

[1] H.H. Xu, X.L. Hu, Y.M. Sun, H.L. Yang, X.X. Liu, Y.H. Huang, Nano Res. 8 (2015) 1148–1158.
[2] C. Xiang, M. Li, M. Zhi, A. Manivannan, N. Wu, J. Power Sources 226 (2013) 65–70.
[3] L. Li, K.H. Seng, Z.X. Chen, H.K. Liu, I.P. Nevirkovets, Z.P. Guo, Electrochim. Acta 87 (2013) 801–808.
[4] L. Huang, J.W. Xiang, W. Zhang, C.J. Chen, H.H. Xu, Y.H. Huang, J. Mater. Chem. A 3 (2015) 22081–22087.

[5] J. Yang, X. Duan, W. Guo, D. Li, H. Zhang, W. Zheng, Nano Energy 5 (2014) 74–81.
[6] J. Pu, F. Cui, S. Chu, T. Wang, E. Sheng, Z. Wang, ACS Sustain. Chem. Eng. 2 (2014) 809–815.
[7] C. Tan, H. Zhang, Chem. Soc. Rev. 44 (2015) 2713–2731.
[8] K. Zhang, Z. Hu, X. Liu, Z. Tao, J. Chen, Adv. Mater. 27 (2015) 3305–3309.
[9] J.L. Yue, Q. Sun, Z.W. Fu, Chem. Commun., Cambridge, U.K., 49, 2013, pp. 5868–5870.
[10] P. Simon, Y. Gogotsi, Nat. Mater. 7 (2008) 845–854.
[11] G. Wang, L. Zhang, J. Zhang, Chem. Soc. Rev. 41 (2012) 797–828.
[12] Q.H. Wang, Y.X. Zhu, J. Xue, X.S. Zhao, Z.P. Guo, C. Wang, ACS Appl. Mater. Interfaces 8 (2016) 17226–17232.
[13] M. Zhi, C. Xiang, J. Li, M. Li, N. Wu, Nanoscale 5 (2013) 72–88.
[14] C. Zhou, Y.W. Zhang, Y.Y. Li, J.P. Liu, Nano Lett. 13 (2013) 2078–2085.
[15] R. Liu, J. Duay, S.B. Lee, Chem. Commun. 47 (2011) 1384–1404.
[16] N. Yu, M.-Q. Zhu, D. Chen, J. Mater. Chem. A 3 (2015) 7910–7918.
[17] A. Banerjee, S. Bhatnagar, K.K. Upadhyay, P. Yadav, S. Ogale, ACS Appl. Mater. Interfaces 6 (2014) 18844–18852.
[18] B. Li, J. Liu, Z. Nie, W. Wang, D. Reed, J. Liu, P. McGrail, V. Sprenkle, Nano Lett. 16 (2016) 4335–4340.
[19] Z. Jiang, W.J. Lu, Z.P. Li, K.H. Ho, X. Li, X.L. Jiao, D.R. Chen, J. Mater. Chem. A 2 (2014) 8603–8606.
[20] Z. Jiang, Z.P. Li, Z.H. Qin, H.Y. Sun, X.L. Jiao, D.R. Chen, Nanoscale 5 (2013) 11770–11775.
[21] Y. Zhao, Z. Song, X. Li, Q. Sun, N. Cheng, S. Lawes, X. Sun, Energy Storage Mater. 2 (2016) 35–62.
[22] Y.Y. Lu, W.W. Zhan, Y. He, Y.T. Wang, X.J. Kong, Q. Kuang, Z.X. Xie, L.S. Zheng, ACS Appl. Mater. Interfaces 6 (2014) 4186–4195.
[23] X. Xu, R. Cao, S. Jeong, J. Cho, Nano Lett. 12 (2012) 4988–4991.
[24] R.B. Wu, X.K. Qian, F. Yu, H. Liu, K. Zhou, J. Wei, Y.Z. Huang, J. Mater. Chem. A 1 (2013) 11126–11129.
[25] H.B. Wu, B.Y. Xia, L. Yu, X.Y. Yu, X.W. Lou, Nat. Commun. 6 (2015) 6512.
[26] W. Meng, W. Chen, L. Zhao, Y. Huang, M. Zhu, Y. Huang, Y. Fu, F. Geng, J. Yu, X. Chen, C. Zhi, Nano Energy 8 (2014) 133–140.
[27] X.M. Zhou, X.T. Shen, Z.M. Xia, Z.Y. Zhang, J. Li, Y.Y. Ma, Y.Q. Qu, ACS Appl. Mater. Interfaces 7 (2015) 20322–20331.
[28] H. Hu, J.T. Zhang, B.Y. Guan, X.W. Lou, Angew. Chem. Int. Ed. 55 (2016) 9512–9516.
[29] H. Hu, B. Guan, B. Xia, X.W. Lou, J. Am. Chem. Soc. 137 (2015) 5590–5595.
[30] R. Banerjee, A. Phan, B. Wang, C. Knobler, H. Furukawa, M. O'Keeffe, O.M. Yaghi, Science 319 (2008) 939–943.
[31] Z. Li, L.X. Yuan, Z.Q. Yil, Y. Liu, Y.H. Huang, Nano Energy 9 (2014) 229–236.
[32] A.C. Ferrari, J. Robertson, Phys. Rev. B 61 (2000) 14095–14107.
[33] H.B. Wang, T. Maiyalagan, X. Wang, ACS Catal. 2 (2012) 781–794.
[34] F. Hao, Y. Yao, Y. Li, C. Tian, X. Zhang, J. Chen, RSC Adv. 5 (2015) 77527–77533.
[35] C.H. Zhang, L. Fu, N. Liu, M.H. Liu, Y.Y. Wang, Z.F. Liu, Adv. Mater. 23 (2011) 1020–1024.
[36] T. Horikawa, N. Sakao, T. Sekida, J. Hayashi, D.D. Do, M. Katoh, Carbon 50 (2012) 1833–1842.
[37] S. Yang, R. Lv, C. Wang, Y. Liu, Z. Song, J. Alloy. Compd. 579 (2013) 628–632.
[38] Y. Du, X. Zhu, X. Zhou, L. Hu, Z. Dai, J. Bao, J. Mater. Chem. A 3 (2015) 6787–6791.
[39] K. Niu, B. Yang, J. Cui, J. Jin, X. Fu, Q. Zhao, J. Zhang, J. Power Sources 243 (2013) 65–71.
[40] Y. Yang, J. Liu, Y. Han, H. Huang, N. Liu, Y. Liu, Z. Kang, Phys. Chem. Chem. Phys. 16 (2014) 25350–25357.
[41] B. Cao, G.M. Veith, J.C. Neuefeind, R.R. Adzic, P.G. Khalifah, J. Am. Chem. Soc. 135 (2013) 19186–19192.
[42] H.W. Liang, W. Wei, Z.S. Wu, X.L. Feng, K. Mullen, J. Am. Chem. Soc. 135 (2013) 16002–16005.
[43] K. Wang, C. Zhou, D. Xi, Z. Shi, C. He, H. Xia, G. Liu, G. Qiao, Nano Energy 18 (2015) 1–11.
[44] F. Zheng, Y. Yang, Q. Chen, Nat. Commun. 5 (2014) 5261.
[45] D. Gueon, J.H. Moon, ACS Appl. Mater. Interfaces 7 (2015) 20083–20089.
[46] X. Xu, M. Wang, Y. Liu, Y. Li, T. Lu, L. Pan, Energy Storage Mater. 5 (2016) 132–138.
[47] B.P. Vinayan, S. Ramaprabhu, J. Mater. Chem. A 1 (2013) 3865–3871.
[48] Y.Y. Li, H.Y. Zhang, Y.M. Chen, Z.C. Shi, X.G. Cao, Z.P. Guo, P.K. Shen, ACS Appl. Mater. Interfaces 8 (2016) 197–207.
[49] K.S.W. Sing, Pure Appl. Chem. 57 (1985) 603–619.
[50] S. Peng, L. Li, H. Tan, R. Cai, W. Shi, C. Li, S.G. Mhaisalkar, M. Srinivasan, S. Ramakrishna, Q. Yan, Adv. Funct. Mater. 24 (2014) 2155–2162.
[51] Y.P. Wang, A.Q. Pan, Q.Y.V. Zhu, Z.W. Nie, Y.F. Zhang, Y. Tang, S.Q. Liang, G.Z. Cao, J. Power Sources 272 (2014) 107–112.
[52] X. Xia, C. Zhu, J. Luo, Z. Zeng, C. Guan, C.F. Ng, H. Zhang, H.J. Fan, Small 10 (2014) 766–773.
[53] H. Jiang, T. Zhao, C. Li, J. Ma, J. Mater. Chem. 21 (2011) 3818–3823.
[54] J. Wen, S. Li, B. Li, Z. Song, H. Wang, R. Xiong, G. Fang, J. Power Sources 284 (2015) 279–286.
[55] H. Jiang, J. Ma, C. Li, Chem. Commun. 48 (2012) 4465–4467.
[56] C. Zhang, H. Yin, M. Han, Z. Dai, H. Pang, Y. Zheng, Y.-Q. Lan, J. Bao, J. Zhu, ACS Nano 8 (2014) 3761–3770.
[57] X. Wang, B. Liu, Q. Wang, W. Song, X. Hou, D. Chen, Y.-B. Cheng, G. Shen, Adv. Mater. 25 (2013) 1479–1486.
[58] B. Wang, J. Park, D. Su, C. Wang, H. Ahn, G. Wang, J. Mater. Chem. 22 (2012) 15750–15756.